Gray-scale photolithography using microfluidic photomasks

Chihchen Chen, Danny Hirdes, and Albert Folch*

Department of Bioengineering, University of Washington, Seattle, WA 98195

Edited by George M. Whitesides, Harvard University, Cambridge, MA, and approved December 23, 2002 (received for review September 23, 2002)

The ability to produce three-dimensional (3D) microstructures is of increasing importance in the miniaturization of mechanical or fluidic devices, optical elements, self-assembling components, and tissue-engineering scaffolds, among others. Traditional photolithography, the most widely used process for microdevice fabrication, is ill-suited for 3D fabrication, because it is based on the illumination of a photosensitive layer through a ''photomask'' (a transparent plate that contains opaque, unalterable solid-state features), which inevitably results in features of uniform height. We have devised photomasks in which the light-absorbing features are made of fluids. Unlike in conventional photomasks, the opacity of the photomask features can be tailored to an arbitrary number of gray-scale levels, and their spatial pattern can be reconfigured in the time scale of seconds. Here we demonstrate the inexpensive fabrication of photoresist patterns that contain features of multiple and/or smoothly varying heights. For a given microfluidic photomask, the developed photoresist pattern can be predicted as a function of the dye concentrations and photomask dimensions. For selected applications, microfluidic photomasks offer a low-cost alternative to present gray-scale photolithography approaches.

Photolithography is used to define critical feature size in the fabrication of the vast majority of microdevices including microelectronic circuits, microelectromechanical systems (MEMS), microfluidic devices, and nucleic acid/protein microarrays (1). Essentially, photolithography consists of selectively illuminating a thin photosensitive layer (''photoresist'') with UV light through a mask containing opaque features (e.g., metal or ink emulsion) on a transparent background (e.g., glass or plastic). The photomasks impose two fundamental limitations on the features that can be produced. (*i*) The exposure is an all-or-none illumination process that results in photoresist features of uniform height; thus, the fabrication of three-dimensional (3D) microstructures by traditional photolithography requires multiple exposure/alignment steps. (*ii*) Photomask features are permanent, and thus design changes require the (costly and slow) fabrication of a new photomask, a major hurdle in research settings requiring fast-turnaround microdevice prototyping.

To overcome the all-or-none illumination constraint of conventional photolithography, a number of ''gray-scale'' approaches capable of generating ranges of exposure levels have been developed. Presently, gray-scale photolithography can be realized with scanning lasers (2, 3), micromirror projection displays (4), high-energy beam-sensitive glass photomasks (www.canyonmaterials.com), ultra-high-resolution ''halftone'' photomasks (5), or metal-on-glass photomasks [where each gray-scale level is determined by a different metal thickness (6)]. Although extremely useful for producing 3D structures, these gray-scale approaches either (*i*) exacerbate the costs/turnaround times of standard photolithography or (*ii*) allow for only a few gray-scale levels. Microlens arrays have been used recently to create inexpensive gray-scale patterns limited to the microlens area ($\approx$100 μm in diameter) (7). Finally, interferometry approaches are capable of producing gray-scale exposures with a limited set of (diffractive) designs (8).

Here we demonstrate a type of gray-scale photomasks that allow for patterning large areas (>3 inches in diameter) using standard photolithographic equipment (i.e., a contact mask aligner with a collimated UV source). Our photomasks contain light-absorbing features that are liquid (i.e., dyes) and can be addressed (i.e., altered) by means of microfluidic channels. We term them ''microfluidic photomasks'' (μFPMs). The μFPMs are advantageous in that (*i*) they contain a virtually unlimited number of gray scales as given by variations in dye concentration, (*ii*) they can be manufactured rapidly and inexpensively, and (*iii*) the fluidic patterns can be changed in the time scale of a few seconds, thus allowing for rapid reconfiguration of the photomask. The μFPMs are sheets of the transparent elastomer polydimethylsiloxane (PDMS) that enclose microfluidic channels. The liquid can be any UV-absorbing water-soluble dye. Our method, schematized in Fig. 1, consists of five steps: (*i*) micropatterning of a silicon master; (*ii*) replica molding of PDMS from the master (9, 10); (*iii*) bonding of the PDMS mold against a PDMS thin film ($\approx$10 μm thick) to form microchannels[†] and introduction of dye solutions of desired concentrations into the microchannels; (*iv*) placing the μFPMs in contact with a photoresist film and exposure of the photoresist to UV light by using standard photolithography equipment [PDMS is convenient because it forms a conformal contact with the photoresist surface (10)]; and (*v*) developing of the photoresist. PDMS is inexpensive, UV-transparent, and replicated from the mold with submicrometer accuracy (9). The fabrication of a μFPM takes <4 h, and both the master and the μFPM can be reused endlessly if handled with care. Elastomeric microfluidic channels filled with dyes have been used previously by Whitesides and coworkers to build reconfigurable diffraction gratings (11).

Materials and Methods

Micropatterning of the Silicon Master. We used transparency masks printed at 5,080 dots per inch (PageWorks, Cambridge, MA). Negative photoresist (SU8-50, MicroChem, Newton, MA) was spun at 500 rpm for 10 s and 2,000 rpm for an additional 30 s, prebaked by ramping up at 4°C/min to 95°C (1 h) with a programmable hot plate (Dataplate Hot Plate/Stirrer Series 730, Barnstead International, Dubuque, IA), and exposed for 150 s with collimated UV light (Kaspar–Quintel Model 2001 aligner; the irradiances at 365, 405, and 436 nm are 0.2, 0.4, and 0.3 mW/cm^2, respectively). After exposure, the SU8 substrate was heated by ramping up at 4°C/min to 95°C (5 min), allowed to cool at the same rate, and developed with SU8 developer (MicroChem) at room temperature for 15 min. For these parameters, the typical feature height was 65 μm. Other heights could be obtained by varying the spinning speed according to the SU8 manufacturer instructions.

This paper was submitted directly (Track II) to the PNAS office.

Abbreviations: μFPM, microfluidic photomask; PDMS, polydimethylsiloxane.

*To whom correspondence should be addressed. E-mail: afolch@u.washington.edu.

[†]The PDMS thin film is not strictly necessary, but it is convenient for making many exposures with the same μFPMs without having to refill the channels. For patterns that require maintaining flow in the microchannel during exposure (e.g., Fig. 2 *D* and *E*), it is more practical to apply the μFPMs directly (without PDMS thin film) on the photoresist.

ENGINEERING

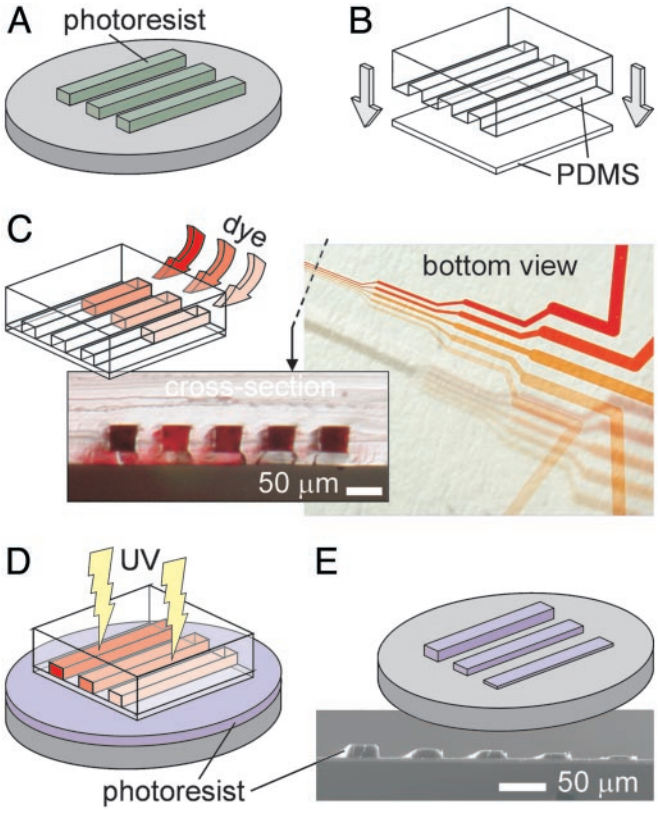

Fig. 1. Fabrication of a μFPM. (*A*) A photoresist micropattern is created on a silicon wafer. (*B*) A PDMS replica of the silicon master is bonded to a spun PDMS thin layer (≈10 μm thick, 4,000 rpm for 30 s). (*C*) The microchannels are filled with dye (Allura red AC, Sigma–Aldrich) at the desired concentrations; the optical micrographs show the bottom view of a μFPM featuring five channels, and its cross section at the location is indicated by a dashed line. (*D*) The μFPM is placed bottom-down onto a spun photoresist film (≈20 μm thick) and exposed to collimated UV light. (*D*) The photoresist is developed. The dye concentrations used to produce the bottom view in *C* do not correspond to the actual concentrations used to create the scanning electron micrograph shown in *E*. For details see *Supporting Text*, which is published as supporting information on the PNAS web site, www.pnas.org.

Replica Molding of PDMS from the Master. A mixture of PDMS prepolymer and curing agent [10:1 (wt/wt), Sylgard 184, Dow-Corning] was cast and cured against the silicon master. To facilitate release, the silicon master was silanized by exposure to a vapor of (tridecafluoro-1,1,2,2,-tetrahydrooctyl)-1-trichlorosilane (United Chemical Technologies, Bristol, PA) in house vacuum at room temperature for 30 min.

PDMS Thin Films. We made 10-μm-thick PDMS films by spinning (4,000 rpm for 30 s) a mixture of PDMS prepolymer (Sylgard 184, Dow-Corning) and hexane [1:3 (wt/wt)] on a 3- to 4-inch-diameter Si wafer. After evaporation of hexane, the film was allowed to cure at 85°C for 3 min on a hot plate. To ensure bonding, we oxidized both PDMS surfaces (the film and the mold) by means of oxygen plasma before bringing them into contact (within 15 min) as described by McDonald *et al.* (10).

Photoresist Micropatterns by Exposure Through μFPMs. Positive photoresist (AZ9260, Clariant, Somerville, NJ) was spun on a 3- to 4-inch-diameter wafer at 500 rpm for 10 s and at 900 rpm for an additional 20 s, then allowed to "relax" for 5 min, prebaked by ramping up at 4°C/min to 90°C (1 h), and ramp-cooled to room temperature at the same rate. An additional relax step of >2 h to avoid cracks was allowed before the 156-s exposure with collimated UV light (Kaspar–Quintel Model 2001 aligner). After exposure, the photoresist was developed for 9 min in AZ400K developer (Clariant) diluted 1:3 (vol/vol) in deionized water. Photoresist heights were measured with a profilometer (Alpha Step 200, Tencor, San Jose, CA).[‡] The photoresist patterns were imaged with a fluorescence microscope (Nikon Diaphot TE300) by using a rhodamine (red-light) emission filter.

Results and Discussion

Gray-Scale Photolithography. Fig. 2 illustrates the variety of photoresist patterns (PR, black-and-white pictures) that can be achieved with μFPMs (color pictures). Photoresist intrinsically fluoresces in red under UV-light stimulation; because higher photoresist patterns fluoresce with brighter intensity, fluorescence brightness images provide a semiquantitative map of the actual topographical height. For quantitative topography measurements we used a profilometer (blue traces in graphs next to images shown in Fig. 2; scale in micrometers). The arrows indicate the direction in which the μFPMs were filled. Higher dye concentrations are designated with arrows of darker red tones and higher numbers (0–5). In Fig. 2*A*, we used a μFPM consisting of five microchannels (Fig. 2*A Upper*), each filled with dye at different concentrations. The topography profile (Fig. 2*A Lower*, blue line) is conveyed qualitatively well by the fluorescence brightness (red line). The close correlation ($r^2 = 0.9868$) between fluorescence intensity and topographical height justifies, for the purpose of this article, the use of fluorescence images to convey photoresist topography. After permutating the dye concentrations, the photoresist pattern changed accordingly (Fig. 2*B*). Hence, contrary to other gray-scale photolithography approaches for which fine-tuning of feature opacity requires the production of a new mask for each design iteration, a μFPM can be reconfigured simply by changing the dye concentration in a given microchannel. We stress that fabrication of the patterns shown in Fig. 2*A* by conventional photolithography, although possible, would have required five different masks, five exposures, and four alignment steps. [Note that the ripples near the walls in Fig. 2 *A–C* are caused by a well studied interference effect in PDMS optical devices (12) and can be avoided by adding glycerol to the dye solution; see the example of nonrippled edges in Fig. 2*D* and, for details, see *Supporting Text*.]

Changing the dye concentration in the μFPMs (either by diffusion or flow) during exposure allows for creating interesting photoresist structures of varying height. When a dye droplet was added to the entrance of microchannels that was already filled with water (Fig. 2*C Left*), dye diffused slowly into the microchannel while the exposure was taking place (Fig. 2*C Center*); this resulted in photoresist "wedges" (Fig. 2*C Right*) oriented along the channel length. To create the structures in Fig. 2 *D* and *E*, dye solutions were flowed during exposure in a μFPM that consisted of five channels merging into one (with the merging point outside of the images to the left). We exploited the fact that typical fluid flows in microchannels are "laminar" (13) (i.e., turbulence and convective mixing are absent): When two or more streams merge, they only mix slowly by diffusion. Laminar flow has been used recently by Whitesides and colleagues to etch and deposit materials inside PDMS microchannels (14). In Fig. 2*D*, alternating streams of dye (5, red arrows) and no dye (0, empty arrows) resulted in photoresist plateaus and valleys, respectively. The valleys are narrower than the plateaus and gradually disappear downstream, because the dye has had time to diffuse into the transparent streams. Thus, Fig. 2*D* also shows that the resolution of our method is not limited by the width of the μFPM channel and provides a way of determining an

[‡]It should be noted that the topography traces are the result of the convolution of the photoresist contour and the contour of the profilometer tip; therefore, walls with a slope higher than that of the tip appear to have the same slope as the tip, and valleys too deep for the tip to reach the bottom appear shallower than they really are.

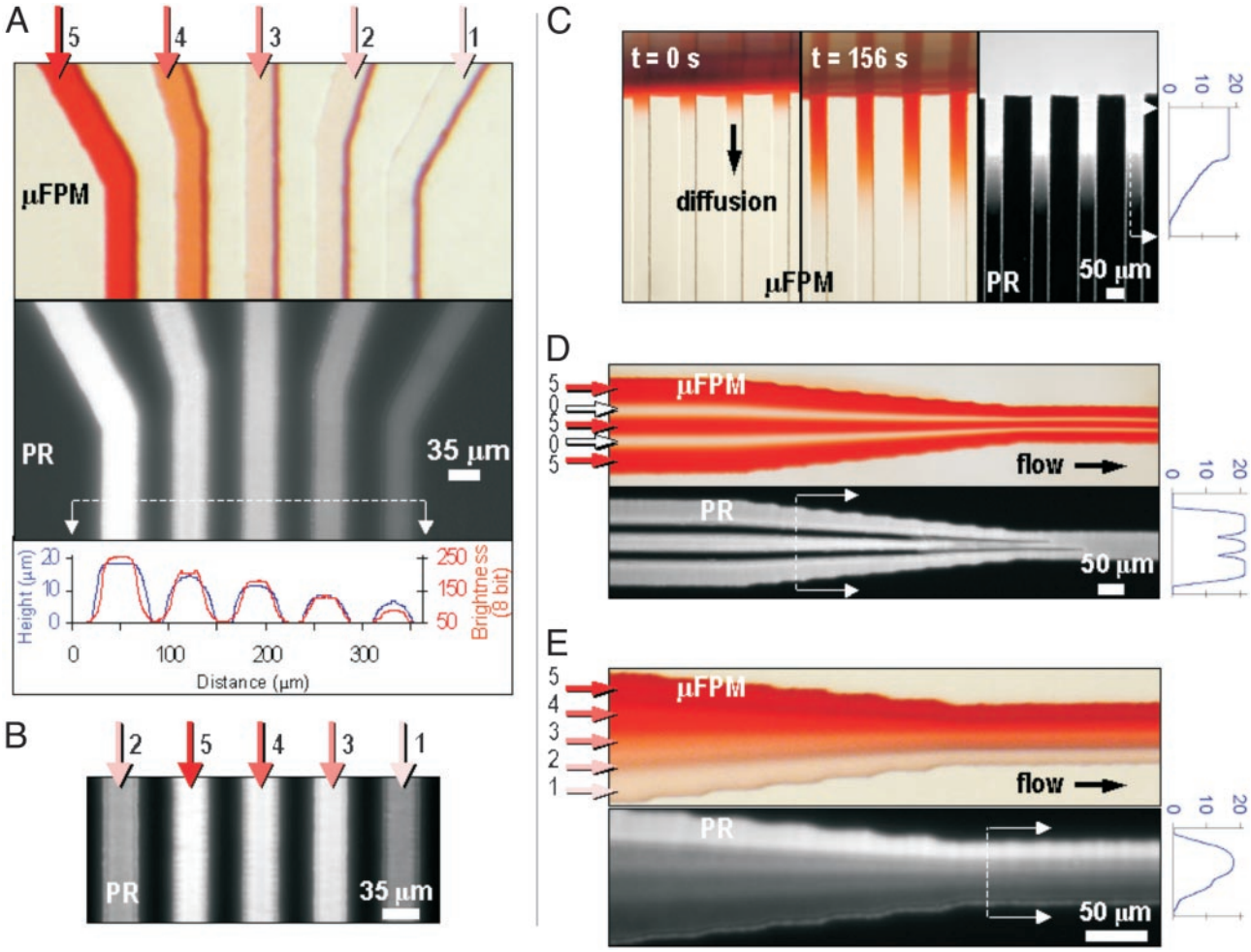

Fig. 2. Various photoresist patterns made with μFPMs. The color images show μFPMs filled with dye, and the black-and-white pictures (PR) are fluorescence micrographs of the photoresist pattern (large fluorescence intensities correspond to large photoresist heights). The blue traces next to the images depict the photoresist profile (in micrometers) at the location indicated by a dashed white line between two arrows. Note that the profilometer tip widens/narrows all sharp contours. The dye concentrations used for the μFPM images were chosen for clarity and do not correspond to the actual concentrations used for producing the photoresist patterns. The μFPM heights, H_L, were 38.9 μm (*A* and *B*), 65.5 μm (*C*), and 67 μm (*D* and *E*). The narrowest portion of the channel in *C* results in a photoresist line that is narrower than the channel, because photoresist gets developed isotropically. In all cases, the dye concentrations, C_d, were adjusted so as to keep the product C_dH_L constant (labeled 5 through 1): 5, 167 mg·cm/liter; 4, 76.6 mg·cm/liter; 3, 62.7 mg·cm/liter; 2, 41.7 mg·cm/liter; and 1, 27.9 mg·cm/liter.

upper-limit value for the resolution (i.e., ≈5 μm for this particular 67-μm-high μFPM).

Multiple streams can also be used to generate dye gradients perpendicular to the direction of the flow (15). To generate the photoresist "staircase" shown in Fig. 2*E*, the same μFPM used for Fig. 2*D* was filled with five dye solutions of decreasing opacity (top to bottom). The sharpness of the steps decreases downstream because of diffusion (15). In principle, the width and position of each stream within the μFPM in Fig. 2 *D* and *E* may be controlled by adjusting the relative flow rates of the confluent streams (14). Automated reconfiguration of fluid flows in microchannels has been demonstrated by using elastomeric microvalves and pumps (16), electrical breakdown of adjacent microchannel walls (17), swelling of polymer parts (18), or electrokinetic valving (19), thus it should be possible to automate μFPM "redrawing" with accurate control systems.

Theoretical Modeling of Exposure Through μFPMs. The final photoresist height can be predicted from the percentage of transmitted light or "transmittance" *T*. PDMS and water are virtually transparent (T = ≈92–93.3% and >99.97%, respectively) at the wavelengths corresponding to the emission lines of the mercury lamp (365, 405, and 435 nm) used for exposing photoresist. Thus at any given point of a μFPM feature, *T* can be described by Beer's Law: $\log T = -\varepsilon C_d H_L$, where H_L is the height of the liquid, and ε and C_d are the absorptivity and concentration of the dye, respectively. Measures of transmittance for H_L = 1 cm of varying concentrations of dye solutions revealed good agreement with Beer's Law (see Fig. 5, which is published as supporting information on the PNAS web site). For a given dye, *T* can be adjusted by varying C_d and/or H_L. We introduced dye at various concentrations in μFPMs of different heights keeping the product C_dH_L in the range of 0–270 mg·cm/liter. For C_dH_L larger than ≈100 mg·cm/liter (corresponding to an average transmittance $T_{avg} < 10\%$), the μFPMs can be considered fully opaque for the exposure and developing times used in this work (156 s and 9 min, respectively); because of the high solubility of the dye, T_{avg} as low as 4×10^{-7} (C_dH_L = 700 mg·cm/liter, corresponding to the "darkest black") can be achieved with 50-μm-high μFPMs. In the range C_dH_L = 0–100 mg·cm/liter (i.e., T_{avg} = 10–100%), we were able to reliably achieve photoresist heights ranging from 0% to 100% of the original unexposed height (see Fig. 6, which is published as supporting information on the PNAS web site), demonstrating that an arbitrarily large number of gray-scale

levels (from transparent to black) can be obtained. In this study, the microchannel heights (≈50 μm) and widths were chosen for ease of operation and fabrication (the transparency masks used for master fabrication are printed at a dot size of ≈5 μm); because we operated at dye concentrations ≈1 order of magnitude below the dye solubility limit (see *Supporting Text*), future higher-resolution masters made with chrome masks could be used to make μFPMs featuring ≈5-μm-deep/wide microchannels while still allowing for a black gray-scale level.

Structures more complex than those shown in Fig. 2 are possible by overlaying μFPMs in multiple exposures. To create the microarray pattern shown in Fig. 3*A*, the same five-channel μFPM (and C_dH_L values) as shown in Fig. 2*A* was used twice subsequently in orthogonal directions. The predicted transmittance pattern (plotted in an inverted 0–255 scale; see *Supporting Text* for details) in Fig. 3*B* is remarkably similar to the fluorescence intensity pattern in Fig. 3*A*. Fig. 3*C* shows that the predictions (Fig. 3*B*) are closely correlated with the average fluorescence brightness (Fig. 3*A*) as well as with the topography (measured at the center of each square). Thus we conclude that Beer's Law gives an accurate prediction of the transmittance through the μFPMs.

Microfluidic Devices Made with μFPMs. As an application, we used μFPMs to address an outstanding problem in microfluidic device fabrication, namely that all the microchannels in a fluidic network (made in the same photolithography step) must have the same height, because in general, they are made by "black-and-white" photolithography (conventional gray-scale photolithography is too expensive to be used for prototype development). The μFPMs allowed us to locally tailor channel height in a single photolithography step, thus introducing a new dimension in microfluidic device design. The microchannels shown in Fig. 4 are made with PDMS replicas of the photoresist structures shown in Fig. 2 *A* and *D*, respectively. Cross-sectional micrographs of the channels along the dashed lines are shown below (Fig. 4*A*) or to the right (Fig. 4*B*) of the dye-filled channels. All five channels shown in Fig. 4*A* were filled with the same blue-dye solution, yet they appear as varying in tone due to differences in channel height. Interestingly, because the photoresist develops isotropically, the microchannels/photoresist patterns have rounded profiles, and shallower lines are narrower. Fig. 4*B* shows three channels (filled with blue, yellow, and red dye) merging into one channel. Note that the photoresist valleys of Fig. 2*D* have resulted, after molding, in PDMS walls separating the three channels upstream. Beyond the merging point, the microchannel walls gradually disappear both in width and in height, a unique geometry that would have been impossible to achieve with conventional photolithography. A growing number of microfluidic applications could benefit from an inexpensive method that allows for producing microchannels of various heights and/or microchannels in which the height varies. For example, present elastomeric valves rely on the bending of the ceiling of the microchannel by an applied pressure (16), and thus a microchannel with a nonuniform height could act as a selective switch by bending differentially along/across the channel. Where real estate is at a premium [e.g., lab-on-a-chip systems (20)], microfluidic mixers that often implement bends in the fluid path to achieve differential fluid-flow resistances could be more compact if the pressure differential were realized by height modulation. In cell-based microchannel bioreactors (21, 22), differences in microchannel height (resulting in different flow rates along the microchannel) could be exploited to generate microflow environments with varying levels of fluid shear stress. Multiheight microchannels could expand the applications of microfluidic molding of polymers (23, 24) and wave guides (25) that are presently limited to structures of regular (usually rectangular) cross section.

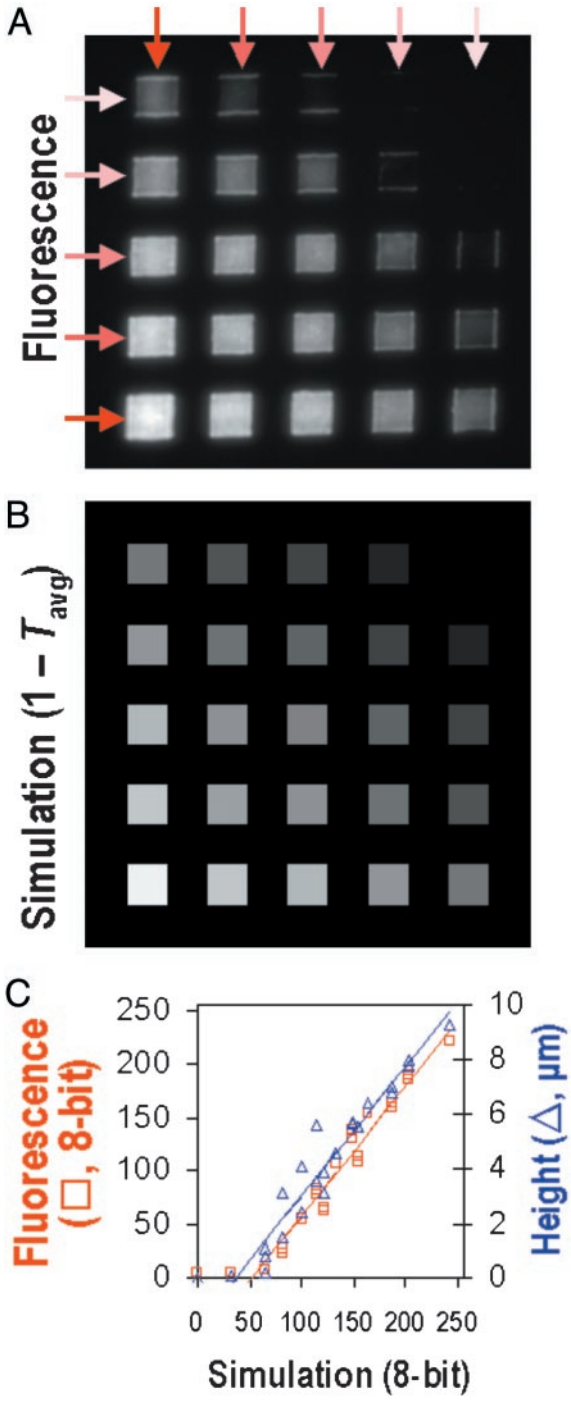

Fig. 3. (*A*) Fluorescence micrograph of a photoresist pattern created by two sequential and orthogonal exposures with the same five-channel μFPM; the same five C_dH_L values described for Fig. 2 were used. (*B*) Eight-bit gray-scale plot of the complement of the transmittances (1 − T_{avg}) averaged over both exposures (78 s each) and the main three UV lamp peak wavelengths (365, 405, and 435 nm); e.g., T_{avg} = 0 and T_{avg} = 1 correspond to 255 (pure white) and 0 (pure black), respectively (see *Supporting Text* for details). (*C*) Plot showing the close correlation between the predicted (1 − T_{avg}) values in *B* and the fluorescence gray-scale data in *A* (red symbols and fitted red line, r^2 = 0.96) and the correlation between (1 − T_{avg}) and the topographical height at the center of the squares in *A* (blue symbols and fitted blue line, r^2 = 0.93).

In conclusion, this work was aimed at demonstrating the fabrication of 3D profiles in photoresist by using fluids as the photomask features. Without attempting to optimize the reso-

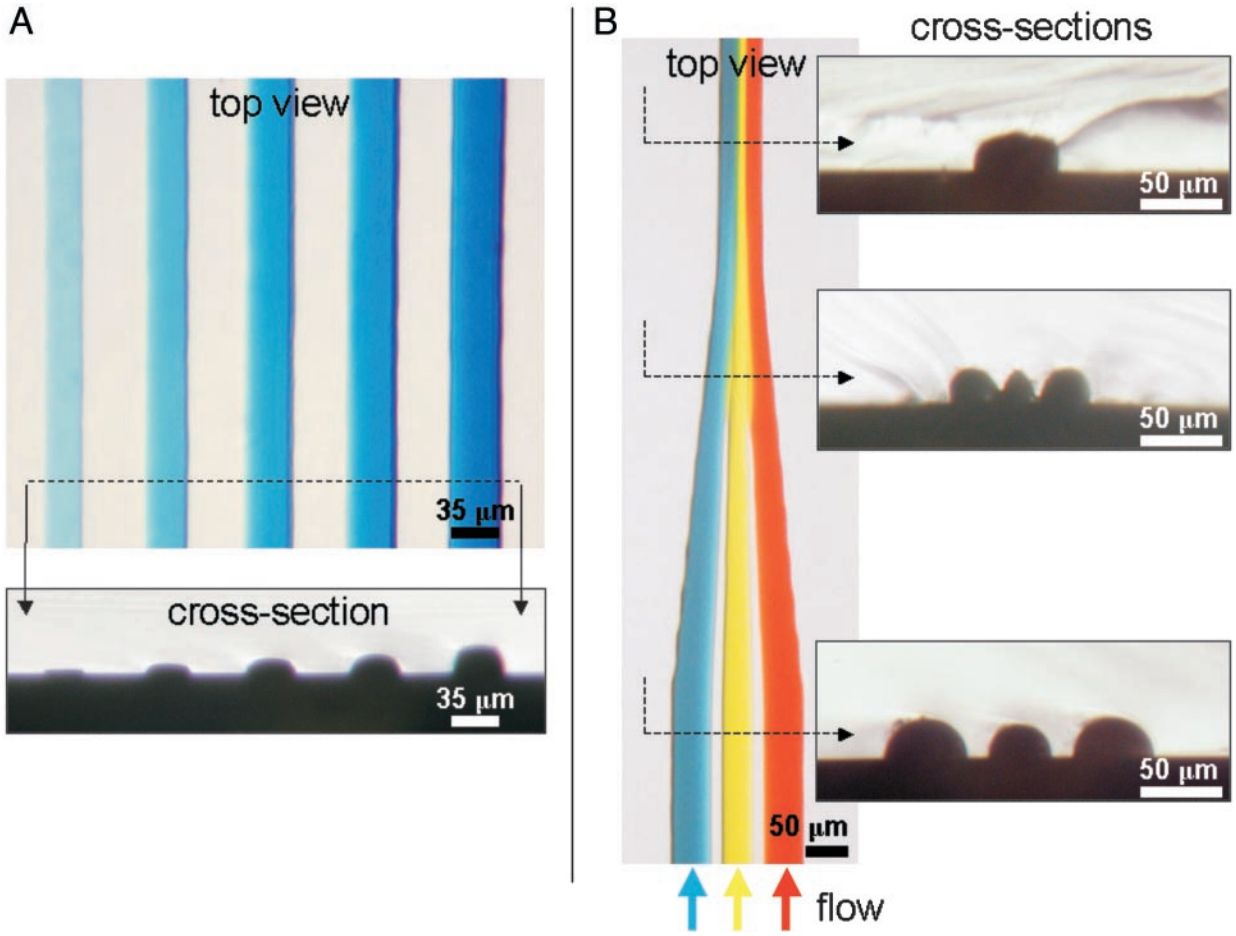

Fig. 4. Microfluidic devices made by PDMS molding against photoresist patterns fabricated in a single exposure with μFPMs. (*A Upper*) Top view of a microfluidic device (PDMS replica of Fig. 2*A*) consisting of five channels (filled with the same blue dye solution) of different height (left to right): 5.4, 7.7, 11.1, 13.4, and 18.1 μm. (*A Lower*) Cross-sectional cut of the PDMS device at the location indicated by the dashed line between the two arrows. (*B Left*) Top view of a microfluidic device (PDMS replica of Fig. 2*D*) consisting of three channels (filled with blue, yellow, and red dyes flowing from bottom to top) merging into one; the streams do not mix readily because of laminar flow (see text). (*B Right*) Three cross-sectional cuts of the PDMS device at the locations indicated by the dashed lines; note how the PDMS walls between the three channels narrow gradually in width (until the channels merge) and height, effectively creating a microtextured channel ceiling (*Middle*).

lution nor account for other adverse effects such as diffraction by the PDMS wall corners, we were able to fabricate patterns that contained 5-μm-sized features. Higher resolution may be achieved by introducing more dye streams into one channel, removing the PDMS thin film, and/or using smaller μFPM heights, dyes of larger molecular weight (i.e., of slower diffusivity), and/or smaller times of residence of the dye in the channel (i.e., higher flow rates). Other methods for creating or manipulating fluid features on surfaces at high resolution by using wettability patterns (26–28) may also find a use in μFPMs.[§] Our method has a few drawbacks compared with other gray-scale photolithography methods. (*i*) Addressing the fluids in the μFPMs places constraints on the sizes and shapes that can be produced (for example, producing isolated features as shown in Fig. 3*B* required two sequential exposures); more complex, 3D microfluidic networks (10, 29–31) should allow for greater pattern-design versatility. (*ii*) Because PDMS is transparent, only clear-field masks are possible at present; in principle, PDMS could be made selectively opaque with the introduction of dyes or particles during molding, or 3D networks with overlapping channels could provide a 100% fill factor. (*iii*) Due to diffusion, the smoothness in gray-scale changes depends on the time of residence of the dye-concentration profile in the channel (i.e., the dye-concentration profiles across the channel under laminar flow vary along the channel length). (*iv*) Filling and/or flushing of the μFPMs may become problematic for applications where the channels need to be narrower, shallower, longer, or more intricate than the ones demonstrated in this work. However, for applications not bound to these constraints (such as the microfluidic devices shown in Fig. 4), the strategy of using photomasks that contain fluidic features provides an enabling alternative to presently available gray-scale-capable photolithographic methods that are comparatively more costly and/or require instrumentation not immediately available in most cleanroom facilities. Because of their intrinsic low cost and fabrication versatility, we believe that our μFPMs have a wide applicability in prototyping of devices containing multiheight microstructures such as microfluidic, micromechanic, or microoptic parts and devices (32).

[§]For example, we have serendipitously found that photoresist turns from highly hydrophobic to very hydrophilic when exposed to a brief (≈5 s) oxygen plasma. When the oxygen plasma exposure was masked with an elastomeric membrane containing holes in intimate contact with the photoresist surface, wettability patterns of dye solution with the same shape as the stencil holes formed onto the photoresist. A quick dip of the photoresist in dye solution resulted in the automatic assembly of microdroplets on the photoresist surface. The dye microdroplets then acted as nonaddressable μFPMs that, after photoresist development, resulted in dome-shaped photoresist structure (data not shown).

We thank Lisa Horowitz and Robert Franza for insightful discussions and Robin Fong and Pat Stayton for the use of the spectrometer. Photolithography was done at the Washington Technology Center (Seattle) facilities. This work was supported by the University of Washington, the Howard Hughes Medical Institute, and the Whitaker Foundation.

1. Madou, M. J. (1997) *Fundamentals of Microfabrication* (CRC, Boca Raton, FL).
2. Bertsch, A., Lorenz, H. & Renaud, P. (1999) *Sens. Actuators A Phys.* **73,** 14–23.
3. Clemence, J. F., Ranieri, J. P., Aebischer, P. & Sigrist, H. (1995) *Bioconjugate Chem.* **6,** 411–417.
4. Sampsell, J. B. (1994) *J. Vac. Sci. Technol. B* **12,** 3242–3246.
5. Wagner, B., Quenzer, H. J., Henke, W., Hoppe, W. & Pilz, W. (1995) *Sens. Actuators A Phys.* **46,** 89–94.
6. Daschner, W., Lon, P., Larsson, M. & Lee, S. H. (1995) *J. Vac. Sci. Technol. B* **13,** 2729–2731.
7. Wu, H., Odom, T. W. & Whitesides, G. M. (2002) *Anal. Chem.* **74,** 3267–3273.
8. Dontha, N., Nowall, W. B. & Kuhr, W. G. (1997) *Anal. Chem.* **69,** 2619–2625.
9. Xia, Y. N. & Whitesides, G. M. (1998) *Angew. Chem. Int. Ed. Engl.* **37,** 551–575.
10. McDonald, J. C., Duffy, D. C., Anderson, J. R., Chiu, D. T., Wu, H. K., Schueller, O. J. A. & Whitesides, G. M. (2000) *Electrophoresis* **21,** 27–40.
11. Schueller, O. J. A., Duffy, D. C., Rogers, J. A., Brittain, S. T. & Whitesides, G. M. (1999) *Sens. Actuators A Phys.* **78,** 149–159.
12. Rogers, J. A., Paul, K. E., Jackman, R. J. & Whitesides, G. M. (1997) *Appl. Phys. Lett.* **70,** 2658–2660.
13. Karniadakis, G. E. & Beskok, A. (2002) *Microflows: Fundamentals and Simulation* (Springer, New York).
14. Kenis, P. J. A., Ismagilov, R. F. & Whitesides, G. M. (1999) *Science* **285,** 83–85.
15. Jeon, N. L., Dertinger, S. K. W., Chiu, D. T., Choi, I. S., Stroock, A. D. & Whitesides, G. M. (2000) *Langmuir* **16,** 8311–8316.
16. Unger, M. A., Chou, H. P., Thorsen, T., Scherer, A. & Quake, S. R. (2000) *Science* **288,** 113–116.
17. McDonald, J. C., Metallo, S. J. & Whitesides, G. M. (2001) *Anal. Chem.* **73,** 5645–5650.
18. Beebe, D. J., Moore, J. S., Bauer, J. M., Yu, Q., Liu, R. H., Devadoss, C. & Jo, B. H. (2000) *Nature* **404,** 588–590.
19. Jacobson, S. C., Ermakov, S. V. & Ramsey, J. M. (1999) *Anal. Chem.* **71,** 3273–3276.
20. Mastrangelo, C. H., Burns, M. A. & Burke, D. T. (1998) *Proc. IEEE J. Microelectromech. Sys.* **86,** 1769–1787.
21. Ledezma, G. A., Folch, A., Bhatia, S. N., Yarmush, M. L. & Toner, M. (1999) *J. Biomech. Eng.* **121,** 58–64.
22. Takayama, S., McDonald, J. C., Ostuni, E., Liang, M. N., Kenis, P. J. A., Ismagilov, R. F. & Whistesides, G. M. (1999) *Proc. Natl. Acad. Sci. USA* **96,** 5545–5548.
23. Kim, E., Xia, Y. N. & Whitesides, G. M. (1995) *Nature* **376,** 581–584.
24. Xia, Y. N., Kim, E. & Whitesides, G. M. (1996) *Chem. Mater.* **8,** 1558–1567.
25. Yang, P. D., Wirnsberger, G., Huang, H. C., Cordero, S. R., McGehee, M. D., Scott, B., Deng, T., Whitesides, G. M., Chmelka, B. F., Buratto, S. K. & Stucky, G. D. (2000) *Science* **287,** 465–467.
26. Abbott, N. L., Folkers, J. P. & Whitesides, G. M. (1992) *Science* **257,** 1380–1382.
27. Abbott, N. L., Gorman, C. B. & Whitesides, G. M. (1995) *Langmuir* **11,** 16–18.
28. Herminghaus, S., Gau, H. & Monch, W. (1999) *Adv. Mater.* **11,** 1393–1395.
29. Anderson, J. R., Chiu, D. T., Jackman, R. J., Cherniavskaya, O., McDonald, J. C., Wu, H. K., Whitesides, S. H. & Whitesides, G. M. (2000) *Anal. Chem.* **72,** 3158–3164.
30. Jo, B. H., Van Lerberghe, L. M., Motsegood, K. M. & Beebe, D. J. (2000) *Proc. IEEE J. Microelectromech. Sys.* **9,** 76–81.
31. Chiu, D. T., Jeon, N. L., Huang, S., Kane, R. S., Wargo, C. J., Choi, I. S., Ingber, D. E. & Whitesides, G. M. (2000) *Proc. Natl. Acad. Sci. USA.* **97,** 2408–2413.
32. Sankur, H. O. & Motamedi, M. E. (2000) *Proc. SPIE Int. Soc. Opt. Eng.* **4179,** 30–55.